Journal of the Korean Society of Surveying, Geodesy, Photogrammetry and Cartography
Vol. 35, No. 4, 319-326, 2017
https://doi.org/10.7848/ksgpc.2017.35.4.319

ISSN 1598-4850(Print)
ISSN 2288-260X(Online)
Original article

COSMO-SkyMed 2 Image Color Mapping Using Random Forest Regression

Seo, Dae Kyo[1] · Kim, Yong Hyun[2] · Eo, Yang Dam[3] · Park, Wan Yong[4]

Abstract

SAR (Synthetic aperture radar) images are less affected by the weather compared to optical images and can be obtained at any time of the day. Therefore, SAR images are being actively utilized for military applications and natural disasters. However, because SAR data are in grayscale, it is difficult to perform visual analysis and to decipher details. In this study, we propose a color mapping method using RF (random forest) regression for enhancing the visual decipherability of SAR images. COSMO-SkyMed 2 and WorldView-3 images were obtained for the same area and RF regression was used to establish color configurations for performing color mapping. The results were compared with image fusion, a traditional color mapping method. The UIQI (universal image quality index), the SSIM (structural similarity) index, and CC (correlation coefficients) were used to evaluate the image quality. The color-mapped image based on the RF regression had a significantly higher quality than the images derived from the other methods. From the experimental result, the use of color mapping based on the RF regression for SAR images was confirmed.

Keywords : Random Forest Regression, Color Mapping, Synthetic Aperture Radar, COSMO-SkyMed 2, WorldView-3

1. Introduction

SAR (Synthetic aperture radar) images are microwave frequency images that provide information about the Earth's surface using wave signals reflected from the observation area (Uhlmann and Kiranyaz, 2014). Compared with optical images, SAR images have higher sensitivity to the backscattering of terrains and objects, are less affected by weather conditions, and can be obtained around the clock. Because of these advantages, SAR images are used in agriculture, forestry, oceanography, geology, as well as in military and natural disaster studies (Uhlmann and Kiranyaz, 2014). However, unlike optical images acquired using visible radiation, SAR images exhibit poor decipherability and studies have focused on color mapping processes to enhance the decipherability of the images (Deng *et al*., 2008). Color mapping studies have included the fusion of SAR images and multispectral images and channel combinations of PolSAR (polarimetric SAR) images (Deng *et al*., 2008; Hong *et al*., 2009). In fusion-based color mapping, the SAR image is used as the panchromatic band and is fused with a multispectral image. In this approach, numerous distortions occur due to the fundamental differences between the two image types (Wang and Chen, 2016). In the channel combination approach for a PolSAR image, decomposition is conducted first based on the scattering mechanism. Subsequently, colors are assigned to the RGB (red, green, and blue) channels. In this method, the colors of the synthesized image are not similar to the colors of an optical image (Deng *et al*., 2008). To overcome these limitations, this study suggests a method

Received 2017. 08. 07, Revised 2017. 08. 19, Accepted 2017. 08. 29
1) Member, Dept. of Smart ICT Convergence, Konkuk University (E-mail: tjeory@konkuk.ac.kr)
2) Member, Dept. of Civil and Environmental Engineering, Seoul National University (E-mail: yhkeen@gmail.com)
3) Corresponding Author, Member, Dept. of Advanced Technology Fusion, Konkuk University (E-mail: eoandrew@konkuk.ac.kr)
4) Agency for Defense Development (E-mail: wypark@add.re.kr)

This is an Open Access article distributed under the terms of the Creative Commons Attribution Non-Commercial License (http://creativecommons.org/licenses/by-nc/3.0) which permits unrestricted non-commercial use, distribution, and reproduction in any medium, provided the original work is properly cited.

for color mapping on the actual pixel values of a SAR image using RF (random forest) regression. RF regression can be modeled with high accuracy as the relationship between two data contain complex information or are non-linear, and has higher accuracy and predictability than other statistical technologies (Rodriquez-Galiano *et al*., 2015). Due to these characteristics, it is expected that modeling of the relationship between SAR images and multispectral images with complex differences such as spectral and acquisition geometry will be performed with high accuracy when using RF regression (Chandrakanth *et al*., 2011).

A SAR image and a multispectral image are selected as input and reference images for the test area. After performing the classification on the reference image, the RF regression for each class is set to obtain the color mapping relationship for the RGB bands. Finally, the obtained color mapping relationship is applied to the SAR image for the color mapping. By comparing the result with images derived from the traditional image fusion method, the applicability of the RF regression is evaluated.

2. Experimental Data

2.1 Test area and data

The test area included the districts of Gwangjin-gu and Seongdong-gu in Seoul. A COSMO-SkyMed 2 image acquired on September 19, 2014 and a WorldView-3 image acquired on August 9, 2015 were used. For the geocoding of the COSMO-SkyMed 2 image, the open source SNAP (Sentinel Application Platform) was used. For the radiometric calibration, the 'calibrate' tool was applied. The image was then converted into square pixels by the 'Multilooking' tool. In addition, to correct the geometric errors that were generated during the acquisition of the SAR image, the 'Range-Doppler Terrain Correction' tool was used for terrain correction. Thereafter, the commercial software ENVI was used to resample the COSMO-SkyMed 2 and WorldView-3 images to a spatial resolution of 2 m and to re-project the coordinates into the WGS84 UTM 52N projection format. The COSMO-SkyMed 2 image and the WorldView-3 image are shown in Figs. 1(a) and (b). And the overall data specifications of study site are described in Table 1.

Table 1. Data specifications

	Worldview-3	COSMO-SkyMed2
Acquisition date	2015.08.09	2014.09.19
Sensor	Woldview-3 sensor(VNIR)	SAR
Spatial resolution(m)	2	2
Image size(pixel)	2500x2500	2500x2500
Acquisition mode	-	HIMAGE

2.2 Speckle noise removal

SAR images invariably include speckle noise. The noise appears as a multiplicative noise in the image. Speckle noise has a granular pattern that affects edge detection and segmentation analyses. Therefore, SAR images must be preprocessed to remove speckle noise (Wang *et al*., 2012). The speckle noise was removed by image filtering, which refers to a method for removing noise by applying a window called a kernel (Ozdarici and Akyurek, 2010). In this study, a Gamma-Map filter, frost filter, lee filter, enhanced frost filter, and enhanced lee filter were used with a window size of 5 x 5. The performances of these filters were evaluated by the ENL

(a) (b)

Fig. 1. Study area: (a) 2014.09.19. COSMO SkyMed2, (b) 2015.08.09. WorldView-3

Fig. 2. COSMO-SkyMed 2 image with speckle noise removed using Gamma-MAP filter

(equivalent number of looks), the SSI (speckle suppression index), the SMPI (speckle suppression and mean preservation index), and the Q (quality factor). The indices are expressed by Eqs. (1), (2), (3), and (4):

$$\text{ENL} = \frac{\mu_{I_t}}{\sigma_{I_t}} \tag{1}$$

$$\text{SSI} = \frac{\sigma_{I_t}}{\mu_{I_t}} \times \frac{\mu_{I_o}}{\sigma_{I_o}} \tag{2}$$

$$\text{SMPI} = (1 + |\mu_{I_o} - \mu_{I_t}|) \times \frac{\sigma_{I_t}}{\sigma_{I_o}} \tag{3}$$

$$\text{Q} = \frac{\mu_{I_o} - |\mu_{I_o} - \mu_{I_t}|}{(\sigma_{I_t}{}^2) \times {\mu_{I_o}{}^2}/{\sigma_{I_o}{}^2}} \tag{4}$$

where μ_{I_o} refers to the mean of the original image, μ_{I_t} to the mean of the filtered image, σ_{I_o} to the standard deviation of the original image, and σ_{I_t} to the standard deviation of the filtered image. In the cases of ENL and Q, higher values indicate a higher performance, while SSI and SMPI exhibit better performances at lower values (Wang *et al*., 2012; Ozdarici and Akyurek, 2010). The Gamma-MAP filter had the highest performance with the following index values: SSI of 0.6937, SMPI of 0.6940, ENL of 10.7143, and Q of 2.0777. Therefore, the Gamma-MAP filter was selected as the speckle noise filter and the noise-free image is shown in Fig. 2.

3. Methods

3.1 Random forest regression

RF regression is an ensemble approach based on the CART (classification and regression tree) method and capable of modeling the relationship between linear and nonlinear dimensions. The more complex the relationship between the data, the higher the accuracy and predictability are (Breiman, 2001; Rodriquez-Galiano *et al*., 2015). The results are obtained by developing multiple trees and averaging the trees. Therefore, the values are not sensitive to statistical abnormality and are highly stable (Prased *et al*., 2006). Here, the training data for each tree are created using a process called bagging (bootstrap aggregating). This means that the training data are created by multiple samplings of the entire data with replacement. Trees formed by bagging are independent; therefore, the error of overfitting is reduced (Breiman, 2001). The performance of the RF regression is evaluated by using a portion of the data excluded from the training, which is called OOB (out-of-bags). In addition, because OOB provides the relative importance of the variables, the interactions between variables can be determined (Gromping, 2009). With high-dimensional data, this information is highly useful (Strobl *et al*., 2008; Rodriguez-Galiano *et al*., 2015).

3.2 Color mapping of the SAR image

The pixel values of the SAR images correspond to the R, G, and B bands as 1:3. This information was used to establish the RF regression equation. Here, the COSMO-SkyMed 2 image is designated as the input image and the WorldView-3 image as the reference image to perform the RF regression. Subsequently, the PIFs (pseudo-invariant features) were extracted to derive the regression equation. PIFs refer to areas in the image where the spectral reflectance barely changes over time and where the pixel values of the identical positions in the two images are thought to exhibit a linear relationship (Caselles and Garcia, 1989). In this study, PCA (principal components analysis) was used. Due to the spectral differences between the COSMO-SkyMed 2 image and the WorldView-3 image, the COSMO-SkyMed 2 image was assumed as gray, while the gray image of WorldView-3 image was obtained to conduct the PCA (Hong *et al*., 2009). The principal component is used to obtain the linear relationship of the bands, while the pixels located on the major axis are selected as the PIFs. Normally, only a limited number of PIFs are extracted; however, in the case of RF regression, a sufficient number of training data are required due to the characteristics of the machine learning algorithm. Therefore, a large number of PIFs were extracted (Du *et al*., 2002; Shaikhina *et al*., 2017). Additionally, to obtain an RF regression for each class, a maximum likelihood classification was performed for the reference image using seven landcover classes, namely water, urban, barren land, forest, grass, shadow, and asphalt.

Eleven parameters were used for the RF regression and they included the GLCM (gray-level co-occurrence matrix)

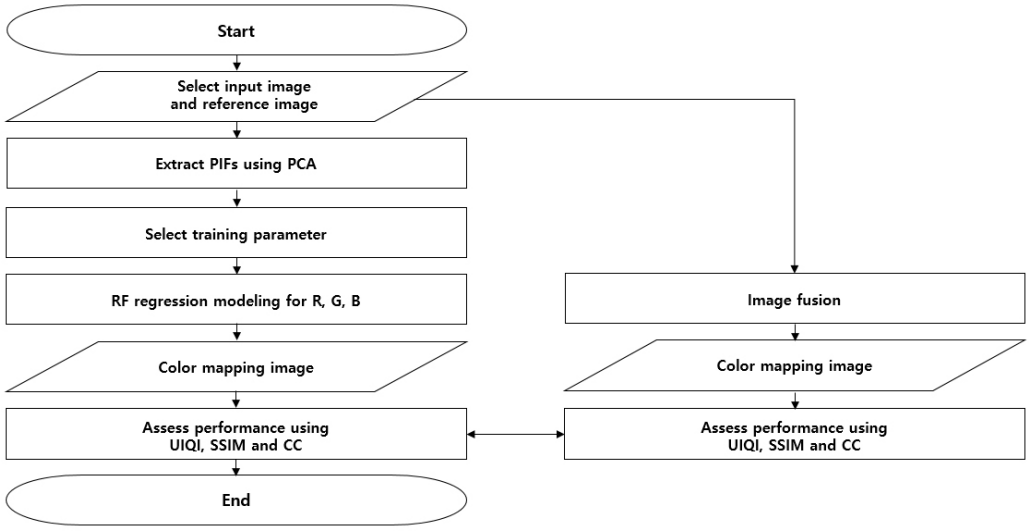

Fig. 3. Experiment flow

texture measures of contrast, dissimilarity, homogeneity, energy, correlation, and ASM (angular second moment) of the COSMO-SkyMed 2 image; the mean, variance, and local contrast-enhanced pixel values; and the edge values based on the Roberts edge detection algorithm. After obtaining the parameters for the extracted PIFs, the RF regressions for B (band 1), G (band 2), and R (band 3) were modeled to conduct the color mapping of the COSMO-SkyMed 2 image. Finally, by comparing the results with those of the image fusion, the applicability of the color mapping approach using RF regression was evaluated. The overall flow of experiment is described in Fig. 3.

3.3 Performance evaluation

To evaluate the image quality of the color-mapped COSMO-SkyMed 2 image, the UIQI (Universal Image Quality Index), SSIM (Structural Similarity) index, and the CC (Correlation Coefficient) were obtained and compared with the indices of the color-mapped image based on image fusion. At this time, UIQI and SSIM are methods of measuring objective image quality based on HVS (Human Visual System), and image quality is measured as the human eye would do. In other words, image quality is measured by extracting different information such as contrast, color, and frequency changes from a visual scene. For this reason, UIQI and SSIM are more accurate and consistent than other image quality measurement methods (Al-Najja and Chen, 2012). The UIQI is calculated by utilizing the combination of luminance, contrast, and structure and the values for the color-mapped image and the reference image can be compared; the UIQI is expressed as shown in Eqs. (5), (6), (7), and (8) (Wang and Bovik, 2002).

$$l(x,y) = \frac{2\mu_x\mu_y}{{\mu_x}^2 + {\mu_y}^2} \tag{5}$$

$$c(x,y) = \frac{\sigma_{xy}}{{\sigma_x}^2 + {\sigma_y}^2} \tag{6}$$

$$s(x,y) = \frac{\sigma_{xy}}{\sigma_x\sigma_y} \tag{7}$$

$$UIQI = l(x,y)\cdot c(x,y)\cdot s(x,y) = \frac{4\mu_x\mu_y\sigma_{xy}}{({\mu_x}^2+{\mu_y}^2)({\sigma_x}^2+{\sigma_y}^2)} \tag{8}$$

where μ_x, μ_y refer to the means of the respective images, σ_x, σ_y refer to the standard deviations of the respective images, and σ_{xy} refers to the covariance of the two images. SSIM is an index for measuring the structural similarity between images based on the human visual system. SSIM is also calculated by combining luminance, contrast, and structure. The respective comparisons and SSIM equations are shown in Eqs. (9), (10), (11), and (12) (Wang *et al*., 2004).

$$l(x,y) = \frac{2\mu_x\mu_y + C_1}{\mu_x^2 + \mu_y^2 + C_1} \quad (9)$$

$$c(x,y) = \frac{2\sigma_x\sigma_y + C_2}{\sigma_x^2 + \sigma_y^2 + C_2} \quad (10)$$

$$s(x,y) = \frac{\sigma_{xy} + C_3}{\sigma_x\sigma_y + C_3} \quad (11)$$

$$SSIM(x,y) = \frac{(2\mu_x\mu_y + C_1)(2\sigma_{xy} + C_2)}{(\mu_x^2 + \mu_y^2 + C_1)(\sigma_x^2 + \sigma_y^2 + C_2)} \quad (12)$$

where C_1, C_2, and C_3 refer to constant values. CC represents the correlation between the two images and is expressed as shown in Eq. (13) (Al-Wassai *et al*., 2011).

$$CC = \frac{\sigma_{xy}}{\sigma_x\sigma_y} \quad (13)$$

The ranges of UIQI, SSIM, and CC are [-1, 1] and a value of 1 indicates the best image quality.

4. Results

For the color mapping of the COSMO-SkyMed 2 image, the COSMO-SkyMed 2 image was selected as the input image and the WorldView-3 image as the reference image. Out of 6,500,000 pixels, 5,206,287 pixels were extracted as PIFs. For the performance evaluation, 33% of the PIFs were used as OOB data. In addition, a maximum likelihood classification was conducted for the reference image so that the RF regression could be applied to each class. The results are shown in Fig. 4. The classification accuracy was 88.3770% and the kappa coefficient was 0.8509.

With respect to the RF regression, 32, 64, and 128 were selected as the number of trees. The test was conducted three times. The image quality of the color-mapped images was evaluated by using UIQI, SSIM, and CC. The performance results are shown in Table 2. With regard to the time required for the test, the use of 32 trees was the most efficient, so we performed color mapping using the regression obtained through 32 trees. The result of the color mapping of the COSMO-SkyMed 2 image is shown in Fig. 5(a). For comparison, a traditional color mapping methods, image fusion, were used on the input and reference images; the Brovey Transform method and modified IHS method were used. In the formal case, it is a simple numerical method that adds intensity and brightness to an image by multiplying normalized multispectral image with high resolution, and it is advantageous to generate an image with superior spatial separation between different objects (Amarsaikhan *et al*., 2010). In the latter case, it is an improvement on the performance of the most commonly used IHS method, and it is advantageous to acquire color mapping image suitable for visual interpretation (Srimani and Prasad, 2014). The color mapping results obtained by image fusion are shown in Figs. 5(b) and (c). Based on a visual analysis, while the color-mapped image based on the RF regression showed features and colors that were similar to the reference image, the images obtained by image fusion were similar the COSMO-SkyMed 2 image even though they were colored. Especially, when comparing extracted region of Figs. 5(a), (b), and (c), the color mapping image acquired through RF regression is easy to distinguish roads and buildings visually, while the

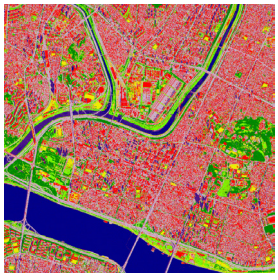

Fig. 4. Classification using maximum likelihood

Table 2. Performance evaluation of RF regression and image fusion

Tree number	Band	UIQI	SSIM	CC	Time
32	Band1	0.6640	0.5743	0.7383	2011.8916
	Band2	0.6404	0.5546	0.7109	
	Band3	0.6281	0.5913	0.6927	
64	Band1	0.6621	0.5722	0.7398	4017.7546s
	Band2	0.6444	0.5579	0.7192	
	Band3	0.6279	0.5978	0.7001	
128	Band1	0.6651	0.5744	0.7399	8056.6456s
	Band2	0.6450	0.5567	0.7201	
	Band3	0.6278	0.5965	0.7004	
Brovey Transform method	Band1	0.1370	0.1358	0.1652	-
	Band2	0.1073	0.0689	0.1278	
	Band3	0.0912	0.1608	0.1073	
Modified IHS method	Band1	0.1269	0.1692	0.1272	-
	Band2	0.1004	0.1198	0.1006	
	Band3	0.0778	0.2132	0.0781	

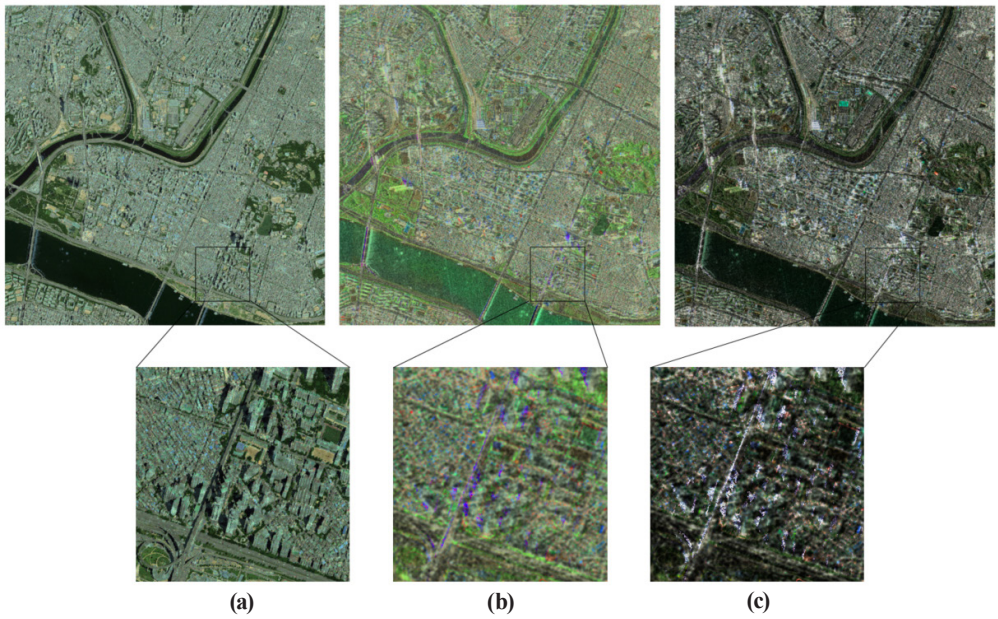

Fig. 5. Color mapping images: (a) derived from RF regression, (b) derived from Brovey Transform method, (c) derived from modified IHS

color mapping image acquired through Brovey Transform and modified IHS show that it is difficult to visually identify roads and buildings. For a quantitative comparison of the performance, the images obtained by image fusion were also used for extracting the UIQI, SSIM, and CC values as shown in Table 2. Compared to the color mapping images obtained by image fusion, the image quality of the color mapping image obtained by RF regression was significantly higher. The Quantitative improvements of RF regression compared with image fusion are shown in Table 3. Therefore, we determined that the RF regression is useful for color mapping of SAR images.

Table 3. Quantitative improvements of RF regression compared with image fusion

Compared method	Band	UIQI	SSIM	CC
Brovey Transform	Band1	0.5270	0.4216	0.6131
	Band2	0.5331	0.4857	0.5831
	Band3	0.5369	0.4305	0.5854
Modified IHS	Band1	0.5371	0.4051	0.6111
	Band2	0.5400	0.4348	0.6103
	Band3	0.5503	0.3781	0.6146

5. Conclusion

In this study, color mapping of SAR images using RF regression was investigated. The image quality was compared with images obtained by image fusion, a traditional color mapping method, by evaluating the UIQI, SSIM, and CC values. Compared with the Brovey Transform, the color mapping image based on RF regression showed higher values of mean UIQI, SSIM, and CC values of 0.5323, 0.4459, and 0.5939, respectively, and higher values of 0.5424, 0.4060, and 0.6120, respectively, when compared with modified IHS. In other words, it was confirmed that the performance of the olor mapping image based on RF regression is significantly higher.

Future studies should focus on enhancing the performance of the RF regression, while also providing additional utility by evaluating a sufficient number of images for different areas, seasons, and periods. Moreover, the applicability of the method should be further investigated by applying the RF regression to SAR images obtained from different satellites.

Acknowledgment

This research was supported by Basic Science Research Program through the NRF (National Research Foundation of Korea) funded by the Ministry of Education (No. 2016R1D1A1B03933562).

Reference

Al-Najja, Y. and Chen, S.D. (2012), Comparison of image quality assessment: PSNR, HVS, SSIM, UIQI, *International Journal of Scientific & Engineering Research*, Vol. 3, No. 8, pp. 1-5.

Al-Wassai, F.A., Kalyankar, N.V., and Al-Zaky, A.A. (2011), The statistical methods of pixel-based image fusion, *International Journal of Artificial Intelligence and Knowledge Discovery*, Vol. 1, No. 3, pp. 1-10.

Amarsaikhan, D., Blotevogel, H.H., van Genderen, J.L., Ganzorig, M., Gantuya, R., and Nergui, B. (2010), Fusing high-resolution SAR and optical imagery for improved urban land cover study and classification, *International Journal of Image and Data Fusion*, Vol. 1, No. 1, pp. 83-87.

Breiman, L. (2001), Random forests, *Machine Learning*, Vol. 45, No. 1, pp. 5-32.

Caselles, V. and Lopez Garrcia, M.J. (1989), An alternative simple approach to estimate atmospheric correction in multitemporal studies, *International Journal of Remote Sensing*, Vol. 10, No. 6, pp. 1127-1134.

Chandrakanth, R., Saibaba, J., Varadan, J., and Raj, P.A. (2011), Feasibility of high resolution SAR and multispectral data fusion, *2011 IEEE International Geoscience and Remote Sensing Symposium*, IEEE, 24-29 July. Vancouver, BC, Canada, Vol. 1, pp. 356-359

Deng, Q., Chen, Y., Zhang, W., and Yang, J. (2008), Colorization for polarimetric SAR image based on scattering mechanisms, *2008 Congress on Image and Signal Processing*, IEEE, 27-30 May, Sanya, Hainan, China, Vol. 5, pp. 697-701.

Du, Y., Teillet, P., and Cihlar, J. (2002), Radiometric normalization of multitemporal high-resolution satellite image with quality control for land cover change detection, *Remote Sensing of Environment*, Vol. 82, No. 1, pp. 123-134.

Gromping, U. (2009), Variable importance assessment in regression: linear regression versus random forest, *The American Statistician*, Vol. 63, No. 4, pp. 308-319.

Hong, G., Zhang, Y., and Mercer, B. (2009), A wavelet and HIS integration method to fuse high resolution SAR with moderate resolution multispectral images, *Photogrammetric Engineering & Remote Sensing*, Vol. 75, No. 10, pp. 1213-1223.

Ozdarici, A. and Akyurek, Z. (2010), A comparison of SAR filtering technique on agricultural area identification, *ASPRS 2010 Annual Conference*, ASPRS, 26-30 April, San Diego, California, unpaginated CD-ROM.

Prasad, A.M., Iverson, L.R., and Liaw, A. (2006), Newer classification and regression tree techniques: bagging and random forests for ecological prediction. *Ecosystems*, Vol. 9, No. 2, pp. 181-199.

Rodriquez-Galiano, V., Sanchez-Castillo, M., Chica-Olmo, M., and Chica-Rivas, M. (2015), Machine learning predictive models for mineral prospectivity: an evaluation of neural networks, random forest, regression trees and support vector machine, *Ore Geology Reviews*, Vol. 71, No. 1, pp. 804-818.

Shaikhina, T., Lowe, D., Daga, S., Briggs, D., Higgins, R., and Khovanova, N. (2017), Decision tree and random forest models for outcome prediction in antibody incompatible kidney transplantation, *Biomedical Signal Processing and Control,* https://doi.org/10.1016/j.bspc.2017.01.012, (last date accessed: 05 August 2017).

Srimani, P.K. and Prasad, N. (2014), Analysis and comparative study of image fusion techniques for land use and land cover classification on Anthrasanthe Hobli, Karnataka, *International Journal of Engineering Research & Technology*, Vol.3, No. 6, pp. 1703-1711.

Strobl, S., Boulesteix, A., Kneib, T., Augustin, T., and Zeileis, A. (2008), Conditional variable importance for random forests, *BMC Bioinformatics*, Vol. 9, No. 307, pp. 1-11.

Uhlmann, S. and Kiranyaz, S. (2014), Integrating color features in polarmetric SAR image classification, *IEEE Transactions on Geoscience and Remote Sensing*, Vol. 52, No. 4, pp. 2197-2216.

Wang, X.L. and Chen, C.X. (2016), Image fusion for synthetic aperture radar and multispectral images based on sub-band-modulated non-subsampled contourlet transform and pulse coupled neural network methods, *The Imaging Science Journal*, Vol. 64, No. 2, pp. 87-93.

Wang, X., Ge, L., and Li, X. (2012), Evaluation of filters for ENVISAT ASAR speckle suppression in pasture area, *ISPRS Annuals of the Photogrammetry, Remote Sensing and Spatial Information Sciences*, ISPRS, 25 August – 01 September, Melbourne, Australia, Vol. l-7, pp. 341-346.

Wang, Z. and Bovik, A.C. (2002), A universal image quality index, *IEEE Signal Processing Letters*, Vol. 9, No. 3, pp. 81-84.

Wang, Z., Bovik, A.C., Sheikh, H.R., and Simoncelli, E.P. (2004), Image quality assessment: from error visibility to structural similarity, *IEEE Transactions on Image Processing*, Vol. 13, No. 4, pp. 600-612.